Protein Science (2000), *9*:1818–1827. Cambridge University Press. Printed in the USA.

Insights into nucleotide binding in protein kinase A using fluorescent adenosine derivatives

DA QUN NI, JENNIFER SHAFFER, AND JOSEPH A. ADAMS

Department of Pharmacology, University of California, San Diego, La Jolla, California 92093-0506

(RECEIVED April 12, 2000; FINAL REVISION June 19, 2000; ACCEPTED June 22, 2000)

Abstract

The binding of the methylanthraniloyl derivatives of ATP (mant-ATP), ADP (mant-ADP), 2′deoxyATP (mant-2′deoxyATP), and 3′deoxyATP (mant-3′deoxyATP) to the catalytic subunit of protein kinase A was studied to gain insights into the mechanism of nucleotide binding. The binding of the mant nucleotides leads to a large increase in fluorescence energy transfer at 440 nm, allowing direct measurements of nucleotide affinity. The dissociation constant of mant-ADP is identical to that for ADP, while that for mant-ATP is approximately threefold higher than that for ATP. The dissociation constant for mant-3′deoxyATP is approximately fivefold higher than that for 3′deoxyATP while derivatization of 2′deoxyATP does not affect affinity. The time-dependent binding of mant-ATP, mant-2′deoxyATP, and mant-ADP, measured using stopped-flow fluorescence spectroscopy, is best fit to three exponentials. The fast phase is ligand dependent, while the two slower phases are ligand independent. The slower phases are similar but not identical in rate, and have opposite fluorescence amplitudes. Both isomers of mant-ATP are equivalent substrates, as judged by reversed-phase chromatography, although the rate of phosphorylation is approximately 20-fold lower than the natural nucleotide. The kinetic data are consistent with a three-step binding mechanism in which initial association of the nucleotide derivatives produces a highly fluorescent complex. Either one or two conformational changes can occur after the formation of this binary species, but one of the isomerized forms must have low fluorescence compared to the initial binary complex. These data soundly attest to the structural plasticity within the kinase core that may be essential for catalysis. Overall, the mant nucleotides present a useful reporter system for gauging these conformational changes in light of the prevailing three-dimensional models for the enzyme.

Keywords: fluorescent nucleotides; protein kinase A; stopped-flow spectroscopy; transient state kinetics

Protein kinases are ATP-dependent enzymes that phosphorylate key proteins in signaling pathways in the cell. The roles of these catalysts have expanded to enormous proportions in recent years. The delivery of a phosphate group from ATP to serine, threonine, or tyrosine side chains in key targets can influence a diverse array of cellular processes including metabolism, mitosis, immune responses, motility, secretion, inflammation, and apotosis. Understanding how these enzymes phosphorylate proteins on a mechanistic level not only is critical for understanding how these cellular processes are regulated but also may provide insights into potential chemotherapeutic strategies. The activities of the protein kinases are tightly regulated through a broad range of mechanisms that include phosphorylation, cellular localization, and protein–protein interactions (Pawson & Scott, 1997). Protein kinases lacking these regulatory components can severely disrupt normal cell function. Indeed, several protein kinases have been linked to human diseases. For example, mutations in the tyrosine kinases, the insulin receptor kinase, Zap 70, and Btk, have been linked to diabetes, severe combined immunodeficiency, and X-linked agammaglobulinemia, respectively (Clauser et al., 1992; Rawlings et al., 1993; Thomas et al., 1993; Chan et al., 1994; Elder et al., 1994). The connection between protein kinases and physiological disorders has prompted the design of inhibitors specific for some of the members in this large enzyme family and clinical trials are underway (Cohen, 1999).

Many protein kinases are structurally complex and composed of one or more noncatalytic domains in addition to a conserved kinase core. The noncatalytic regions are normally involved in activity regulation and/or subcellular localization (Liu & Pawson, 1994; Pawson & Scott, 1997). There are presently a number of

Reprint requests to: Joseph A. Adams, Department of Pharmacology, University of California, San Diego, La Jolla, California 92093-0506; e-mail: joeadams@chem.ucsd.edu.

Abbreviations: C-subunit, catalytic subunit of PKA; HPLC, high-performance liquid chromatography; Kemptide, peptide sequence LRRASLG; mant, the N-methylanthraniloyl moiety; mant-ATP, 2′(3′)-O-(N-methylanthraniloyl) adenosine 5′-triphosphate; mant-ADP, 2′(3′)-O-(N-methylanthraniloyl) adenosine 5′-diphosphate; mant-2′deoxyATP, 3′-O-(N-methylanthraniloyl) 2′deoxyadenosine 5′-triphosphate; mant-3′deoxyATP, 2′-O-(N-methylanthraniloyl) 3′deoxyadenosine 5′-triphosphate; PKA, cAMP-dependent protein kinase.

X-ray structures for the kinase domains and together they define a common structural motif for the enzyme family. The kinase domain of protein kinase A (PKA), the first in the family to be elucidated by X-ray diffraction methods (Knighton et al., 1991a, 1991b), is composed of two subdomains: a small, nucleotide binding domain rich in β structure, and a large substrate binding domain dominated by α-helices. The active site is positioned between these two subdomains and contains several conserved residues predicted to be important for substrate and ATP binding and phosphoryl transfer. The delivery of the phosphoryl group does not occur in the absence of a critical metal activator, Mg^{2+}. This metal chelates the $\beta\gamma$ phosphates of ATP, presumably supporting nucleotide binding and catalysis (Zheng et al., 1993a). The active site also binds a second Mg^{2+}, which has meaningful but complex effects on the steady-state kinetic parameters (Cook et al., 1982; Adams & Taylor, 1993). While the second Mg^{2+} is a nonessential modulator of catalysis, about 1/5 of the sites that bind this metal are occupied at physiological concentrations of 0.5 mM free metal (Cook et al., 1982). The partial population of this secondary metal site is, therefore, significant from a functional perspective.

The mechanism by which protein kinases phosphorylate their protein targets has been under investigation for quite some time, but it has been the more recent applications of solvent perturbation and rapid-mixing techniques that have provided a focused glimpse into the discrete steps associated with catalysis. Viscosometric studies on PKA demonstrated initially that phosphoryl transfer is not a rate-limiting element in turnover (Adams & Taylor, 1992). Rapid quench flow studies were later used to isolate the phosphoryl transfer step (500 s^{-1}) and show that its rate is 20-fold higher than turnover (Grant & Adams, 1996). The slow step in the mechanism has been presumed to be ADP release owing to the low K_d for this product compared to the phosphopeptide (Cook et al., 1982; Bhatnagar et al., 1983), and recent catalytic trapping studies support this presumption (Zhou & Adams, 1997). In these latter experiments, preequilibration of PKA with ADP prior to reaction initiation with ATP and peptide substrate leads to acute "burst" phase attenuation, consistent with rate-determining ADP dissociation (25 s^{-1}). These findings are compatible with the kinetic sequence in Scheme 1 under conditions of saturating ATP concentrations.

The pathway in Scheme 1 was determined when both of the metal sites were occupied with Mg^{2+}. In comparison, pre-steady-state kinetic analyses at 0.5 mM free Mg^{2+}, a physiological level of metal, challenges the simple view for substrate phosphorylation depicted in Scheme 1. Under these conditions, two conformational changes—one prior to and one subsequent to the phosphoryl transfer step—are the primary rate-limiting steps for substrate turnover (Shaffer & Adams, 1999a, 1999b). Both solution and crystallographic models of PKA incorporate flexible segments in the kinase core that may underlie these observations. For example, PKA has been crystallized in either an "open" or "closed" form based on relative movements of the two domains (Zheng et al., 1993b). This movement appears to occur in solution based on small angle X-ray scattering studies (Olah et al., 1993). In addition to these large domain movements, it is likely that changes in several key loop segments are essential for ATP binding based on chemical cleavage studies (Cheng et al., 1998b).

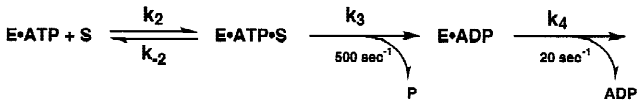

Scheme 1.

It is clear that conformational changes in PKA occur in solution under thermodynamic conditions and some of these changes could be critical for controlling the phosphorylation mechanism. Nonetheless, there is still no link between any structural changes observed under equilibrium conditions and those detected under normal catalytic cycling. Furthermore, it is unclear whether ligand binding, either ATP or peptide, drives these structural changes. For example, PKI causes a decrease in the enzyme's radius of gyration (Olah et al., 1993), yet ATP, and not PKI, alters the susceptibility of the kinase core to chemical cleavage agents (Cheng et al., 1998b). Whatever the source, a more thorough kinetic investigation of the role of structural changes is useful for providing this essential link. To probe further the role of conformational changes in the kinetic mechanism, we investigated the binding of several fluorescent nucleotides to the catalytic subunit of PKA using equilibrium and stopped-flow fluorescence spectroscopy. In particular, because methylanthraniloyl (mant) derivatives of ATP have been used effectively for the study of molecular motors including myosin head fragments, dynein, and kinesin (e.g., Ma & Taylor, 1997; Friedman et al., 1998; Mocz et al., 1998; Moyer et al., 1998), we wondered whether these derivatives would be useful for studying the kinetic mechanism of PKA. In this present study, we demonstrated that mant-ATP is a substrate for PKA and the binding of these derivatives leads to an increase in fluorescence resonance energy transfer. Once bound, the nucleotide–enzyme complex can isomerize to a low fluorescence form. A second conformational change step is important for binding, but it may occur either before or after the initial association complex. These results indicate that mant derivatization of ATP and ADP provides a useful probe for the characterization of conformational changes in PKA.

Results

Fluorescence spectra of mant nucleotide derivatives

Figure 1A displays the spectra of mant-ATP excited at 290 nm in the absence and presence of PKA. The binding of PKA to the nucleotide leads to a large fluorescence increase at 440 nm (approximately twofold enhancement). The spectra for PKA alone are also displayed in Figure 1A. However, only a small amount of fluorescence above 400 nm is observed due to the intrinsic fluorescence of PKA (1 μM) so that the large enhancement at 440 nm upon mant-ATP binding cannot be explained by contributions from the enzyme spectrum. Similar spectra were recorded for the other mant derivatives and, in all cases, a large increase in fluorescence is observed at 440 nm upon the association of the nucleotide and enzyme (data not shown). To determine whether this fluorescence increase is due to an energy transfer process, the spectrum of mant-ATP, excited at 340 nm in the absence and presence of PKA, was recorded. As shown in Figure 1B, no increase in fluorescence is observed, suggesting that the large increase at 440 nm in Figure 1A is due to resonance energy transfer between the protein and the mant fluorophore. A 15% increase in fluorescence at 440 nm was observed upon mixing mant-ADP (120 μM) and PKA (1 μM) using 340 nm excitation (data not shown), suggesting that a small portion of the energy transfer signal for this nucleotide may be due to general environmental factors.

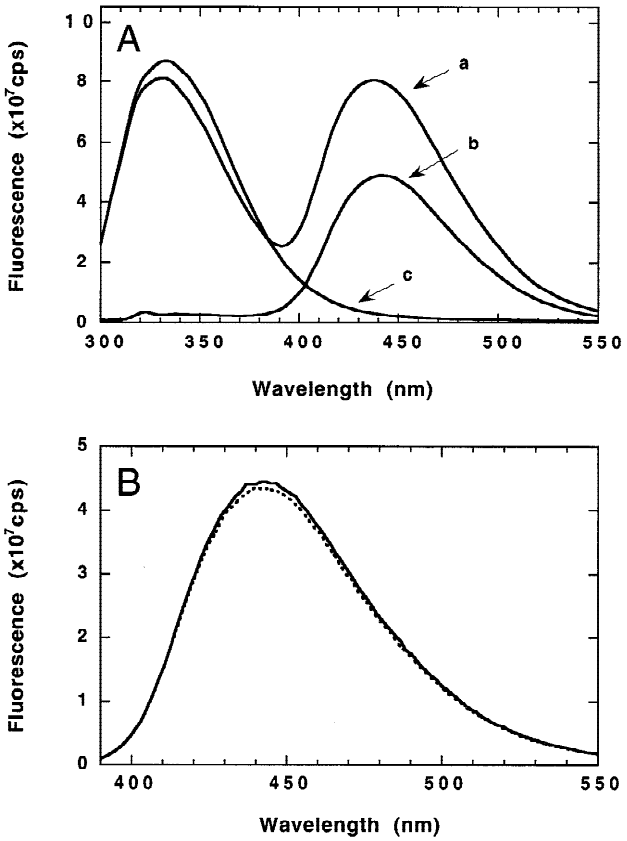

Fig. 1. Fluorescence spectra of mant-ATP in the presence and absence of PKA. **A:** Spectra of mant-ATP with PKA (a), mant-ATP alone (b), and PKA alone (c) upon excitation at 290 nm. The excitation and emission slits are set at 5 nm. **B:** Spectra of mant-ATP with PKA (- - -) and mant-ATP alone (——) upon excitation at 340 nm. The excitation and emission slits are set at 1 nm. The concentrations of mant-ATP, PKA, and $MgCl_2$ are 120 μM, 1 μM, and 10.1 mM, respectively, in all spectra. The fluorescence output is expressed in units of cps (counts per second).

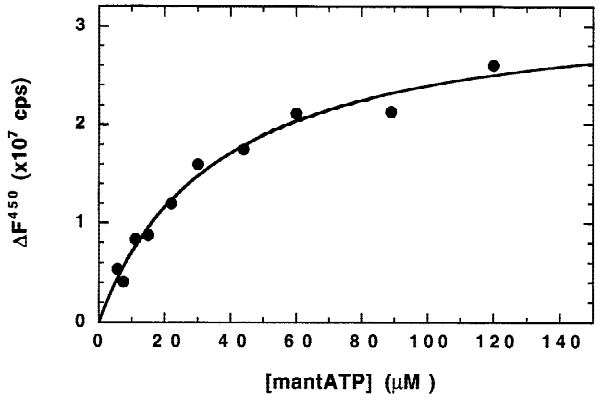

Fig. 2. Change in fluorescence energy transfer as a function of total mant-ATP concentration. The spectra of PKA and mant-ATP alone were subtracted from the spectra of mant-ATP with PKA and the change in fluorescence at 450 nm (ΔF^{450}) was plotted as a function of total mant-ATP concentration (8–120 μM) using 1 μM PKA in all spectra. The fluorescence output is expressed in units of cps (counts per second). The data were fit to a hyperbolic function to obtain a K_d of 36 ± 5 μM.

Dissociation constants of mant nucleotide derivatives

The dissociation constants for the mant nucleotide derivatives were measured using the energy transfer signal resulting from enzyme association. In these experiments, spectra were recorded for mant nucleotides in the absence and presence of PKA, and the changes in fluorescence at 450 nm were measured. This wavelength was selected because very little enzyme fluorescence is detected in this region. Nonetheless, changes in fluorescence at 450 nm upon PKA binding were corrected for the minor contribution of enzyme fluorescence. The change in fluorescence at 450 nm (ΔF^{450}) upon binding mant-ATP is shown in Figure 2. The data are fitted to a hyperbolic function to obtain a K_d of 36 μM for mant-ATP. The fluorescence for mant-ATP in the absence of PKA increased linearly with the concentration of nucleotide (data not shown) so that the curvature in the plot of Figure 2 is not due to saturation of the detector. Binding isotherms were also measured for the other nucleotide derivatives, and the results of the data fits are displayed in Table 1. The nucleotides bind with dissociation constants in the range of 8 to 36 μM.

Phosphorylation of a peptide substrate by PKA using mant-ATP

The ability of mant-ATP to serve as a phosphoryl donor in the PKA-catalyzed reaction was assessed using HPLC detection methods. In this study, PKA (2.5 μM) was allowed to phosphorylate the peptide substrate, GRTGRRNSI (400 μM), using mant-ATP(130 μM). After various time periods, the reaction was acid quenched, and the entire mixture was injected onto the HPLC column. A chromatogram for the reaction after 30 s is shown in Figure 3A. The peaks for mant-ATP, mant-ADP, and peptide were assigned based on injecting purified samples alone onto the HPLC column (data not shown). The mant-ATP sample, which purifies as a single peak on the DEAE sepharose column, appears as a doublet of peaks on the reversed-phase column (arbitrarily assigned peaks #1 and #2). We presume that these peaks correspond to the two

Table 1. *Dissociation constants for mant-nucleotides to PKA using equilibrium fluorescence measurements at 10 mM free Mg^{2+}*[a]

Nucleotide	K_d (μM)	Nucleotide	K_I (μM)
mant-ATP	36 ± 7	ATP	12[b]
mant-ADP	9.0 ± 4	ADP	10[c]
mant-2′deoxyATP	34 ± 10	2′deoxyATP	38[d]
mant-3′deoxyATP	7.6 ± 2.4	3′deoxyATP	1.5[d]

[a]The K_d values were determined by fitting the corrected changes in fluorescence at 450 nm as a function of total nucleotide concentration to a rectangular hyperbolic function. All measurements were made in 50 mM Mops (pH 7) at 25 °C.

[b]This value is based on the K_I of 12 μM for $\beta\gamma$ methylene ATP (Armstrong et al., 1979a) and falls within the limits of ≤15 μM for the K_d of ATP derived from viscosity measurements (Adams & Taylor, 1992).

[c]This value was taken from Shaffer and Adams (1999b).

[d]These values were taken from Hoppe et al. (1978).

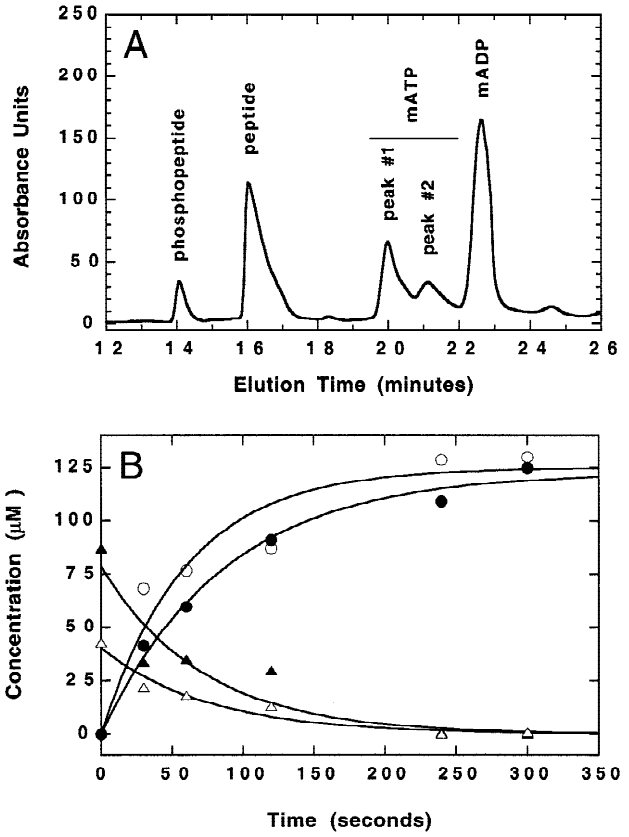

Fig. 3. Time course for the phosphorylation of the peptide substrate GRTGRRNSI using mant-ATP and PKA. **A:** HPLC chromatogram of the components of the phosphorylation reaction. PKA (2.5 μM), mant-ATP (130 μM), and GRTGRRNSI (400 μM) were mixed and allowed to react for 30 s before stopping the reaction with 30% acetic acid. The peaks for peptide, mant-ATP, and mant-ADP were identified by injecting these samples alone (data not shown). The phosphopeptide peak was identified by running the reaction with ATP and monitoring the time-dependent production of this peak (data not shown). **B:** Changes in the concentration of phosphopeptide (●), mant-ADP (○), and peaks #1 (▲) and #2 (△) as a function of time. For this time course, PKA (2.5 μM), mant-ATP (130 μM), and peptide (400 μM) were incubated for varying time periods and then quenched with acetic acid. The peaks from the HPLC chromatograms were integrated, and the areas were converted to concentration based on the initial concentrations of the components. The data were fit to single exponential functions to obtain rates of 0.017, 0.012, 0.014, and 0.013 s^{-1} for the production or disappearance of mant-ADP, phosphopeptide, peak #1, and peak #2, respectively. The total production of phosphopeptide and mant-ADP is 124 μM, while peaks #1 and #2 are 87 and 43 μM prior to reaction.

isomers for the nucleotide, namely 2′ and 3′ mant-ATP (Hiratsuka, 1983). Reinjecting peak #1 onto the HPLC column leads to a doublet of peaks with the same retention time and distribution as the original two peaks (data not shown), confirming this presumption. The peak for mant-ADP may be a doublet, although this cannot be well resolved using this separation system. Simultaneous detection at 356 nm confirms that peaks #1 and #2 and the assigned mant-ADP peak contain the mant fluorophore (data not shown). We identified the phosphopeptide peak by running a control reaction using the natural nucleotide, ATP. With time, a peak that comigrates with that in Figure 3A appears while the peptide peak disappears (data not shown). Both ATP and ADP elute in the void volume of the column (data not shown).

The production and consumption of all reactants and products were followed as a function of time in Figure 3B. The peaks for phosphopeptide and mant-ADP increased as a function of time, while those for mant-ATP decreased with time. The concentrations were determined based on percent integrated areas using 214 nm detection and the known initial concentrations of peptide and mant-ATP. The data were fit to single exponential functions to obtain rate constants for the time-dependent change in species. As shown in the legend of Figure 3, the production of mant-ADP and phosphopeptide and the disappearance of peaks #1 and #2 follow similar rate constants (0.012–0.017 s^{-1}). The concentrations of mant-ADP and phosphopeptide approach 130 μM, the limiting amount of mant-ATP used in these experiments. Because peaks #1 and #2 are not ideally separated in the chromatograms, the largest errors in the depletion of these peaks is expected. Nonetheless, both mant-ATP peaks decreased to zero after 3 min (data not shown) indicating that both isomers are substrates for the enzyme. Finally, the observed rates for substrate depletion and product consumption are approximately 10-fold faster than the isomerization rate for the mant group at the 2′ and 3′ positions of ATP at pH 7 (Cheng et al., 1998a). This indicates that both isomers are utilized directly as substrates rather than an alternative reaction pathway in which one isomer is catalytic and complete turnover awaits the isomerization of the remaining inactive isomer. Based on the initial velocity for the production of phosphopeptide (v = 0.12 $s^{-1} \times 130$ μM = 1.6 μM/s), an observed initial rate constant of 0.64 s^{-1} ($v/[E]$ = 1.6 μM/s/2.5 μM) can be calculated. This rate constant is approximately 20-fold lower than k_{cat} using ATP as a phosphoryl donor (Adams & Taylor, 1992; Shaffer & Adams, 1999b; Zhou & Adams, 1997).

Stopped-flow binding of the mant nucleotide derivatives

The kinetics of nucleotide binding were measured using stopped-flow fluorescence spectroscopy. In these experiments, PKA was mixed with the mant nucleotides in the instrument cuvet and time-dependent changes in fluorescence above 420 nm were recorded upon excitation at 290 nm. As shown in Figure 4A, the binding of mant-ATP (200 μM) to PKA (0.5 μM) is accompanied by three fluorescence changes: a large, rapid (580 s^{-1}) increase followed by a slower increase (40 s^{-1}) and decrease (35 s^{-1}). The inset in Figure 4A shows the first 30 ms of the reaction. The data were also fit using a double exponential equation (dotted line), but this did not provide adequate fitting for data above 30 ms. Also, the fluorescence intensity did not change after 500 ms and up to 10 s, indicating that the slower phases are not the result of photobleaching (data not shown). The triphasic character was also observed at other concentrations of mant-ATP. Figure 4B shows the dependence of the rates of these phases on the total concentration of mant-ATP. The rate of the fast phase (λ_1) increases linearly as a function of the nucleotide concentration while the rates of the second (λ_2) and third (λ_3) phases are not affected by mant ATP within the concentration range studied. The slope (λ_1^{slope}) and intercept values (λ_1^{int}) for λ_1 along with the average values of λ_2 (λ_2^{ave}) and λ_3 (λ_3^{ave}) are displayed in Table 2. The binding of mant-ADP is also accompanied by fast and slower increases followed by a slower decrease in fluorescence (data not shown). The data fitting for these transients is also displayed in Table 2.

To determine whether these kinetic transients are due to isomeric impurities in the mant-ATP samples, the binding of mant-2′deoxyATP was monitored. In this experiment, shown in Figure 5A,

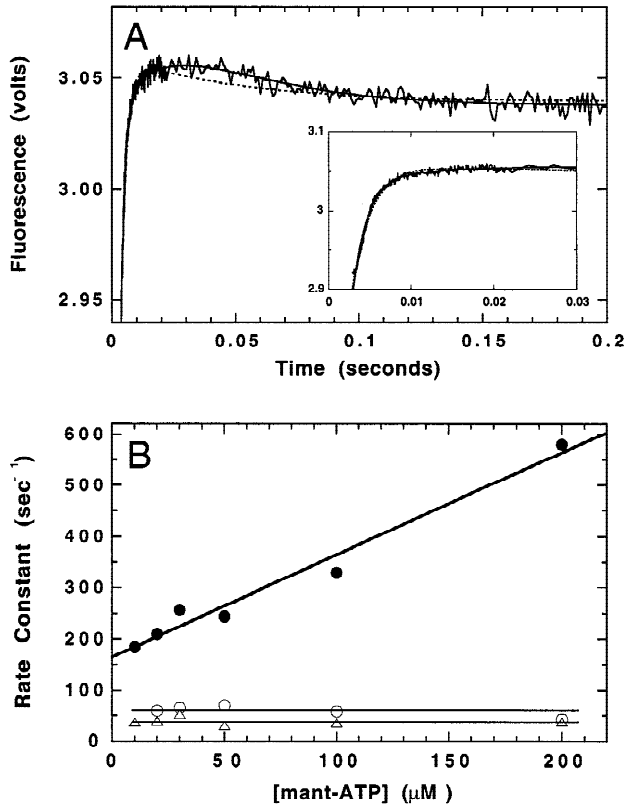

Fig. 4. Binding of mant-ATP to PKA using stopped-flow spectroscopy. **A:** Time-dependent change in fluorescence upon mixing PKA (0.5 μM) and mant ATP (200 μM). Fluorescence signal is collected above 420 nm using a cutoff filter, and the sample is excited at 290 nm. Two sets of 200 data points are collected over two time frames: 0–20 ms and 20–220 ms. A 1.5 ms offset is inserted in the time axis to account for instrument deadtime. The inset shows the first 30 ms of the reaction. The solid line represents a triple exponential fit to the data with the following rate (λ_1, λ_2, λ_3) and amplitude (α_1, α_2, α_3) parameters: $\lambda_1 = 580 \pm 20\ s^{-1}$, $\lambda_2 = 40 \pm 8\ s^{-1}$, $\lambda_3 = 35 \pm 7\ s^{-1}$, $\alpha_1 = 0.82 \pm 0.04$ V, $\alpha_2 = 0.50 \pm 0.02$ V, and $\alpha_3 = -0.49 \pm 0.03$ V. The dotted line represents a double exponential fit to the data with the following rate (λ_1, λ_2) and amplitude (α_1, α_2) parameters: $\lambda_1 = 420 \pm 20\ s^{-1}$, $\lambda_2 = 20 \pm 6\ s^{-1}$, $\alpha_1 = 0.52 \pm 0.02$ V, and $\alpha_2 = -0.021 \pm 0.001$ V. **B:** Effects of total mant-ATP concentration (10–200 μM) on λ_1 (●), λ_2 (○), and λ_3 (△). The fits to the data are presented in Table 2.

PKA (0.5 μM) is mixed with mant-2′deoxyATP (200 μM) in the stopped-flow instrument and the time-dependent change in fluorescence is recorded. The inset in this figure shows the first 30 ms. The binding of this nucleotide derivative to PKA occurs in three phases: a fast increase in fluorescence (510 s^{-1}) followed by a slower increase (50 s^{-1}) and a fluorescence decrease (41 s^{-1}). This transient is similar to that observed for mant-ATP. The fluorescence intensity did not change after 500 ms and up to 10 s, indicating that the second phase is not the result of photobleaching (data not shown). Figure 5B displays the effects of total mant-2′deoxyATP concentration on the rates of both phases. The data were fit identically to that in Figure 4A, and the results are listed in Table 2. There is no difference, within experimental error, in the kinetic parameters for binding mant-ATP or mant-2′deoxyATP, indicating that the multiphase character of nucleotide association and unique opposing fluorescence amplitudes are not due to isomer impurity.

Table 2. *Stopped-flow kinetic parameters for the binding of nucelotides to PKA at 10 mM free Mg^{2+}* [a]

Ligand	λ_1^{slope} ($\mu M^{-1} s^{-1}$)[b]	λ_1^{int} (s^{-1})[b]	λ_2^{ave} (s^{-1})	λ_3^{ave} (s^{-1})
mant-ATP	2.0 ± 0.30	165 ± 25	54 ± 10	39 ± 8
mant-ADP	1.3 ± 0.20	170 ± 15	33 ± 8	27 ± 5
mant-2′deoxyATP	1.5 ± 0.20	220 ± 25	40 ± 14	30 ± 7

[a] Parameters were measured under pseudo-first-order conditions where $[L] > [E]$ in 50 mM Mops (pH 7) at 25 °C.
[b] λ_1^{slope} and λ_1^{int} represent the slope and *y*-intercept terms for the linear dependence of λ_1 on ligand concentration.

Dissociation rate constants for the mant derivatives

The dissociation rate constants for the mant-nucleotides were measured in trapping experiments in the stopped-flow instrument. In these experiments, PKA is preequilibrated with a mant-nucleotide (L) and then mixed rapidly with an equal volume of a trapping ligand (T) in excess amounts ($[T] > [L]$). Time-dependent changes in fluorescence can be monitored if the preequilibrated enzyme–ligand complex has different fluorescence properties then the enzyme-trapping ligand complex. A representative trapping experiment is shown in Figure 6. In this experiment, the displacement of mant-ATP from the enzyme by ATP results in a biphasic fluorescence decrease with rate constants of 190 (λ_1) and 30 (λ_2) s^{-1}. The amplitude of the second phase is considerably smaller than that for the first phase (0.27 vs. −0.018 V). Reducing the concentration of ATP by twofold did not affect these rate constants indicating that the observed values represent limits for the observed dissociation for mant-ATP (data not shown). The same procedure was used to measure the dissociation rate constant for the other mant nucleotides. These values are displayed in Table 2. In all cases, the observed dissociation rate constants are independent of the trapping ligand concentration, a prerequisite for the assignment of the kinetic transients to true "off" rates. For trapping mant-ADP and mant-2′deoxyATP, a second, slow phase was not observed.

Discussion

Binding properties of the fluorescent nucleotides

The binding of the mant nucleotide derivatives to PKA can be monitored owing to a strong fluorescence energy transfer signal at 440 nm (Fig. 1). The dissociation constants for mant-2′deoxyATP and mant-ADP are identical to those for the nonconjugated nucleotides, while the dissociation constant for mant-3′deoxyADP is fivefold higher than that for 3′deoxyADP. Based on the binding of the nonhydrolyzable analog, $\beta\gamma$ methylene ATP (Armstrong et al., 1979b), and viscosometric studies (Adams & Taylor, 1992), the K_d for ATP is expected to be 12 μM, a value threefold lower than that for mant-ATP. Care must be taken in evaluating the K_d values for mant-ATP and mant-ADP. The constants for mant-ATP and mant-ADP represent apparent values because the mant group can reside on either the 2′ or 3′ position, and it is unclear from these measurements whether one or both of the isomers causes fluorescence changes. Nonetheless, the observation that mant-2′deoxyATP and mant-3′deoxyATP cause fluorescence enhancements and bind well

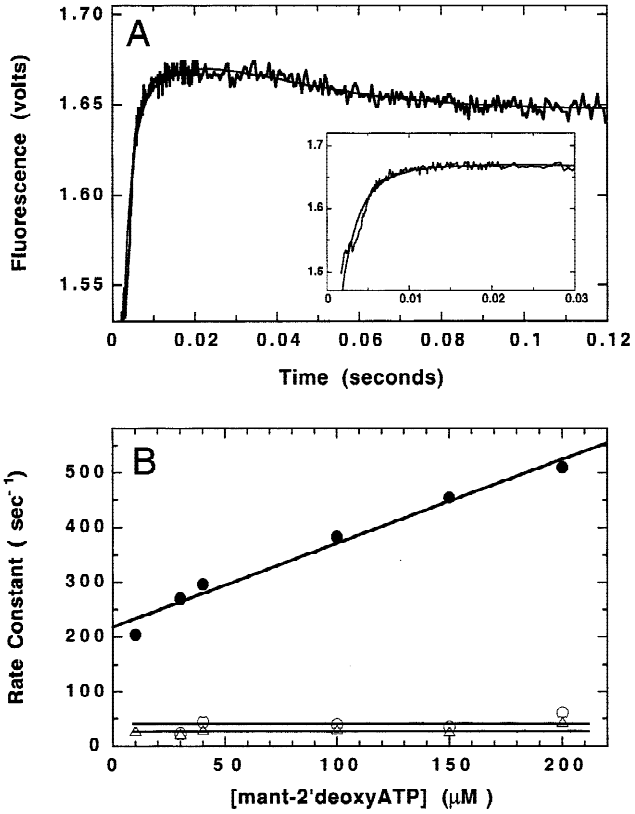

Fig. 5. Binding of mant-2′deoxyATP to PKA using stopped-flow spectroscopy. **A:** Time-dependent change in fluorescence upon mixing PKA (0.5 μM) and mant-2′deoxyATP (200 μM). Fluorescence signal is collected above 420 nm using a cutoff filter, and the sample is excited at 290 nm. Two sets of 200 data points are collected over two time frames (0–20 ms and 20–120 ms). A 1.5-ms offset is inserted in the time axis to account for instrument dead time. The inset shows the first 30 ms of the reaction. The data were fit to a triple exponential function with the following rate (λ_1, λ_2, λ_3) and amplitude (α_1, α_2, α_3) parameters: $\lambda_1 = 510 \pm 30$ s^{-1}, $\lambda_2 = 50 \pm 11$ s^{-1}, $\lambda_3 = 41 \pm 6$ s^{-1}, $\alpha_1 = 0.48 \pm 0.005$ V, $\alpha_2 = 0.25 \pm 0.07$ V, and $\alpha_3 = -0.24 \pm 0.09$ V. **B:** Effects of total mant-2′deoxyATP concentration (10–200 μM) on λ_1 (●), λ_2 (○), and λ_3 (△). The fits to the data are presented in Table 2.

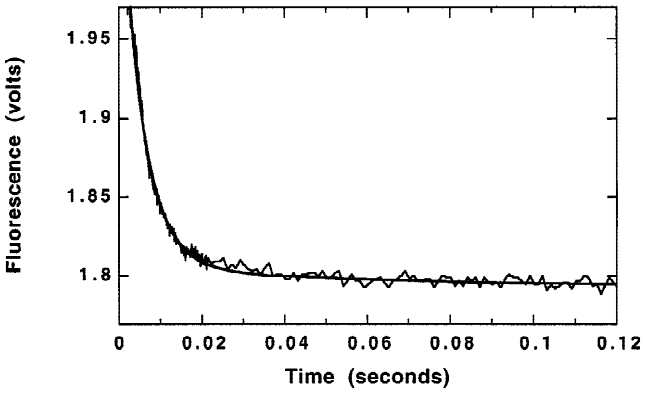

Fig. 6. Trapping mant-ATP from the binary enzyme complex using ATP. PKA (2 μM) is preequilibrated with mant-ATP (400 μM) in one syringe and rapidly mixed with ATP (6,000 μM) in the other syringe. The final concentrations of PKA, mant-ADP, and ATP in the reaction cuvet of the stopped-flow instrument are 1, 200, and 3,000 μM, respectively. Two sets of 200 data points were collected over two time frames—20 and 200 ms (only the first 120 ms is displayed). The data were fit to a double exponential function to obtain rate constants of 190 ± 10 s^{-1} ($\alpha_1 = -0.27 \pm 0.003$ V) and 20 ± 5 s^{-1} ($\alpha_2 = -0.018 \pm 0.002$ V).

compared to the nonderivatized forms suggests that both isomers of mant-ATP bind to PKA (Table 1). In the next two sections, we will provide kinetic evidence to support this claim.

Mant-ATP is a substrate for PKA

Large alterations to the structure of ATP can impair catalytic function. For example, the ATP analogs, lin-benzo-ATP and etheno-ATP, are substrates for PKA but display k_{cat}/K_m values that are 5- and 3,500-fold lower, respectively, than that for the natural nucleotide (Hartl et al., 1983). To assess the viability of mant-ATP as a phosphoryl donor in the PKA-catalyzed reaction, the phosphorylation of the peptide, GRTGRRNSI, was monitored using HPLC methods. This peptide is the best, known substrate for PKA with a k_{cat}/K_m value of $\sim$150 μM^{-1} s^{-1} (Mitchell et al., 1995), a value that is almost two orders of magnitude higher than the traditional substrate, Kemptide (LRRASLG). The phosphorylation of GRTGRRNSI was followed so that the fate of the peptide and the nucleotide could be identified. The chromatograms (Fig. 3) show clearly the time-dependent production of phosphopeptide and mant-ADP peaks as well as the disappearance of the two peaks for mant-ATP. These data demonstrate not only that mant-ATP is a substrate for PKA but also that the two isomers are utilized in the reaction. This supports the previous supposition from the data in Table 1 that both isomers bind to PKA. Also, the similar time constants for the disappearance of peaks #1 and #2 indicate that PKA does not discriminate between the two isomers. Nonetheless, the rate for peptide phosphorylation is approximately 20-fold lower than that observed under identical concentrations of ATP, indicating that mant-ATP is a poor donor in the reaction compared to the natural nucleotide.

Binding mechanism for the mant nucleotides

While the equilibrium fluorescence measurements (Fig. 2; Table 1) provide dissociation constants for the mant derivatives, they do not furnish information regarding the mechanism for nucleotide association. For the binding of mant-ATP and mant-ADP to PKA, the time-dependent changes in fluorescence energy transfer, measured in the stopped-flow instrument, are triphasic. Because the rates of the slower phases (λ_2 and λ_3) do not increase as a linear function of either mant-ATP or mant-ADP and the binding of mant-2′deoxyATP, an analog that is substituted at only one position of the ribose ring, observes multiphasic kinetics (Figs. 4, 5), the triphasic character of the transient state kinetics is due to a minimal, three-step binding mechanism where two of the steps represent conformational changes in the protein. While the ligand dependence on λ_1 indicates that the fast phase corresponds to the bimolecular association event, the position of this step with respect to both conformational changes is uncertain. Because one of the conformational change steps must occur after ligand binding to account for the negative amplitude of λ_3, two mechanistic possibilities, displayed in Schemes 2 and 3, are operative.

In both mechanisms, the isomeric mixtures in mant-ATP and mant-ADP are ignored because similar values for λ_1^{slope} are de-

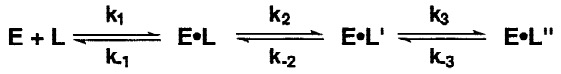

Scheme 2.

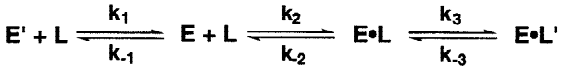

Scheme 3.

tected for all nucleotides (Table 2), the ligand-dependent portions of the binding transients are fit adequately by a single exponential (Table 2), and both isomers of mant-ATP can phosphorylate the peptide substrate at equivalent rates (Fig. 3). Qualitatively, these two mechanisms can explain the transient state data if the fluorescence output for $E \cdot L$ and $E \cdot L'$ exceeds that for $E \cdot L''$ in Scheme 2 or if the fluorescence output for $E \cdot L$ exceeds that for $E \cdot L'$ in Scheme 3.

While mathematical treatments for one- and two-step binding mechanisms are known and reported in several reviews (e.g., Johnson, 1992; Fierke & Hammes, 1995), there is no general analytical solution for a three-step binding mechanism. Nonetheless, approximate solutions can be obtained if the rates of the individual phases are well separated ($\lambda_1 > \lambda_2 > \lambda_3$) or if the initial phase is faster than the second and third phase ($\lambda_1 > \lambda_2, \lambda_3$) (Bernasconi, 1976). The data in Table 2 are most consistent with the latter condition, but the inability to measure a clear hyperbolic ligand dependence on λ_2 and λ_3 prohibits a unique solution to the mechanism in Scheme 2 (Bernasconi, 1976). Regardless, the fast phase slope (λ_1^{slope}) and intercept (λ_1^{int}) are close in value to k_1 and k_{-1}, and provide an estimate of the affinity for the initial enzyme–ligand encounter. Based on viscosity and isotope partitioning studies, k_{cat}/K_{ATP} represents the association rate constant for ATP (Kong & Cook, 1988; Adams & Taylor, 1992). The similarities between k_{cat}/K_{ATP} (1–2 $\mu M^{-1} s^{-1}$) and λ_1^{slope} (Table 2) indicate that the latter is truly measuring the association rate constant for mant-ATP, and that mant derivatization does not impair nucleotide access to the binding pocket. While $\lambda_1^{int}/\lambda_1^{slope}$ is close to K_d for mant-ATP, this ratio is more than 10-fold larger than the K_d for mant-ADP (Tables 1, 2), implying that the conformational change step(s) in the latter mant nucleotide make(s) larger contributions to affinity. Mathematical treatments of complex binding mechanisms predict hyperbolic ligand dependencies on the observed rates of the conformational steps if they are thermodynamically favorable (Bernasconi, 1976; Johnson, 1992). While it is predicted that this would apply to mant-ADP, the inability to measure λ_2 or λ_3 beneath 10 μM ligand makes it difficult to fit a hyperbolic relationship and extract individual rate constants.

Trapping the mant derivatives using ATP

Trapping studies can be helpful for the description of ligand binding to a protein and analytical solutions of ligand dissociation are available for one- and two-step mechanisms (Johnson, 1992; Torok & Trentham, 1994). For a two-step process, double exponential transients may be observed that describe the net decomposition of both ligand-bound complexes. However, monophasic displacement transients may be observed, depending on the relative concentrations of the bound species and their relative fluorescence properties (Torok & Trentham, 1994). Despite the complex kinetic behavior of mant nucleotide binding presented herein (Table 2), the trapping of these ligands occurs in two phases for mant-ATP and only one phase for mant-ADP and mant-2′deoxyATP (Table 3). We interpret these results to mean that the initial encounter of the fluorophore with PKA yields a highly fluorescent species (i.e., $E \cdot L$ in Scheme 2 or 3) that may isomerize to poorly fluorescent forms (i.e., $E \cdot L''$ in Scheme 2 or $E \cdot L'$ in Scheme 3). Indeed, fluorescence decreases are observed for all mant nucleotides indicating that, at least, one of the isomerization steps produces a weakly fluorescent species. Under these conditions, the initial trapping phase reflects primarily the net rate for decomposition of the initial encounter species. For mant-ATP and mant-2′deoxyATP, the initial trapping phase rate (λ_f) is close in value to (λ_1^{int}), suggesting that *EL* in Scheme 2 or 3 is highly fluorescent compared to the isomerized complexes. The low amplitude for λ_s for mant-ATP and the absence of secondary phases for mant-2′deoxyATP and mant-ADP are consistent with weak fluorescence outputs for some of the isomerized forms of PKA in Scheme 2 or 3. While the fluorescence output for $E \cdot L'$ may be greater than $E \cdot L$ in Scheme 2 to account for the positive amplitude for λ_2 (Fig. 4), the lower fluorescence of $E \cdot L''$ compensates for this increase and masks the expected phase for this step in the trapping experiment.

Structural changes induced by the γ phosphate of ATP

Although mant has no effect on ADP binding, fluorophore derivatization of ATP reduces binding affinity by approximately threefold (Table 1). This result suggests that the γ phosphate of ATP induces unique structural changes in the enzyme that influence the ribose portion of the binding pocket. In contrast, X-ray models of PKA with either ATP or ADP bound exhibit no detectable changes in either local or global structure (Madhusudan et al., 1994). Although these contrasting results could mean that fluorophore sensitivity to protein conformation surpasses the limits of crystallographic resolution, the mant results may also imply that the X-ray models for PKA are not entirely representative of solution structures. In addition, other data hint to differences in ATP and

Table 3. *Dissociation rate constants for various nucleotides determined from trapping studies in 10 mM free Mg^{2+}* [a]

Complex[b]	Trapping ligand[c]	λ_f (s^{-1})	λ_s (s^{-1})	$\alpha_s/(\alpha_f + \alpha_s)$[d]
E·mant-ATP	ATP	190 ± 10	20 ± 6	0.07
E·mant-ADP	ATP	75 ± 5		
E·mant-2′deoxyATP	ATP	240 ± 20		

[a] Experiments were performed in a stopped-flow instrument in 50 mM Mops (pH 7) at 25 °C. The fluorescent transients were fit to either single or double exponential functions to give rate constants λ_f and/or λ_s.

[b] Protein–ligand complex preequilibrated in one syringe of the instrument prior to mixing with the trapping ligand.

[c] Ligand used to monitor release of preequilibrated ligand.

[d] $\alpha_s/(\alpha_f + \alpha_s)$ is the ratio of the absolute amplitude of the slow phase (α_s) with respect to the total, absolute amplitude change ($\alpha_f + \alpha_s$).

ADP binding modes. Although energy transfer appears to be the sole mechanism for the observed increases in fluorescence output upon mant-ATP binding (Fig. 1), the fluorescence increases upon mant-ADP binding have a larger solvent component coupled with energy transfer (see Results). Such a result could indicate that mant-ADP adopts a different binding mode than mant-ATP. Furthermore, the inability to closely correlate the observed trapping rate for mant-ADP with λ_1^{int} as had been done in the cases of mant-ATP and mant-2′deoxyATP (Tables 2, 3) suggests that this nucleotide may utilize a more complex binding mechanism than mant-ATP.

Enzyme plasticity and catalysis

In another study from our laboratory, we identified two conformational changes associated with ATP and ADP binding to a fluorescently labeled mutant of PKA (Lew et al., 1997). In this study, an asparagine-to-cysteine mutation in the C-terminal tail was labeled with the fluorophore, acrylodan, creating a mutant enzyme (Acr-N326C) whose fluorescence emission above 400 nm is sensitive to nucleotide binding. The rates for one of the conformational changes (70 s^{-1}) and the bimolecular release step for ADP measured in a trapping experiment (100 s^{-1}) could account for k_{cat} (40 s^{-1}), suggesting that the structural event plays a noticeable role in rate limitation. Although this study was performed on a mutant enzyme with slightly altered steady-state kinetic parameters, the parallels between these results and those for the mant nucleotides are striking. Although the mant and acrylodan fluorophores in both studies are uniquely located in the structure of PKA, both incorporate conformational changes. These parallels, along with the close relationship between the rates of the conformational steps for mant-ADP binding (λ_2^{ave} and λ_3^{ave} in Table 2) and k_{cat} (20 s^{-1}), suggest that structural changes in PKA may play a role in limiting turnover. At a minimum, the data in this manuscript report a high level of enzyme plasticity that may be important for catalysis and may underlie some of the structural heterogeneity observed in X-ray and solution models (Olah et al., 1993; Zheng et al., 1993b; Narayana et al., 1997). The mant derivatives are thus effective tools for relating dynamic ligand processes with three-dimensional models and for defining the contribution of unimolecular, conformational events. Changes in the number or rates of these conformational steps upon selective amino acid replacement will help to link movements in loop or secondary structural elements with nucleotide accommodation in the active site.

Materials and methods

Materials

Adenosine diphosphate (ADP), adenosine triphosphate (ATP), 2′deoxyATP, 3′deoxyATP, 3-(N-morpholino) propane sulfonic acid (Mops), lactate dehydrogenase, pyruvate kinase, nicotinamide adenine dinucleotide, reduced (NADH), and phosphoenolpyruvate were purchased from Sigma Chemicals (St. Louis, Missouri). N-methylisatoic anhydride was purchased from Molecular Probes (Eugene, Oregon). Triethylamine, acetonitrile, trifluoroacetic acid (TFA), and magnesium chloride were purchased from Fisher (Fair Lawn, New Jersey). DEAE Sepharose was purchased from Amersham Pharmacia Biotech (Piscataway, New Jersey).

Peptides and enzyme

The substrate peptides, GRTGRRNSI and LRRASLG, were synthesized at the USC Microchemical Core Facility using Fmoc chemistry and purified by C-18 reversed-phase HPLC. Substrate concentrations were determined by turnover with the C-subunit under conditions of limiting peptide in the spectrophotometric assay. Recombinant C-subunit was expressed in *Escherichia coli*, and purified according to previously published procedures (Yonemoto et al., 1991). The total concentration of the protein was measured by its absorbance at 280 nm ($A_{0.1\%} = 1.2$).

Enzyme assay

The enzymatic activity of the C-subunit was determined as described previously (Cook et al., 1982). The oxidation of NADH, monitored spectrophotometrically as an absorbance decrease at 340 nm, is coupled to the production of ADP by lactate dehydrogenase and pyruvate kinase. All reactions were measured in a Beckman DU640 spectrophotometer equipped with a microcuvet holder. Typical steady-state kinetic assays were performed in 50 mM Mops (pH 7) in a final volume of 60 μL at 24 °C. The active concentration of enzyme was obtained by measuring the intial velocity of the reaction using 3 mM ATP, 0.5 mM LRRASLG and 10 mM free Mg^{2+} assuming a turnover number of 20 s^{-1} at 10 mM free Mg^{2+} (Grant & Adams, 1996).

Preparation of fluorescent nucleotide derivatives

The mant derivatives of ATP, ADP, 2′deoxyATP, and 3′deoxyATP were synthesized and purified using previously published procedures (Hiratsuka, 1983; Woodward et al., 1991). A 1:1.5 molar ratio of nucleotide to methylisatoic anhydride were allowed to react for 2 h at 38 °C, checking the pH to 9.6 with NaOH. The pH was dropped to 7 with HCl, and the reaction mixture was frozen prior to separation. The thawed samples were eluted from a DEAE Sepharose column using a linear gradient of 5 to 900 mM triethylamine-carbonate buffer (pH 8.5). The derivatized nucleotides were well resolved from the underivatized nucleotides and mant groups. The former was identified by the absence of an absorption peak above 300 nm, and the latter was identified by an absorption maximum at 330 nm. The labeled nucleotides were confirmed by the characteristic absorbances at 250 and 356 nm. For the derivatized nucleotides, the ratios of absorbances at 250 and 356 nm (A^{250}/A^{356}) were greater than 3.5, confirming that a single mant group was attached to each nucleotide.

HPLC detection of substrate phosphorylation

The phosphorylation of the peptide substrate, GRTGRRNSI, by PKA using mant-ATP was monitored using HPLC detection. In this assay, PKA (0.1–5 μM), mant-ATP (130–200 μM), and peptide (400 μM) were allowed to react in 3 mL of 50 mM Mops (pH7) at 25 °C. Aliquots (400 μL) were removed at varying time periods (0–300 min) and 25 μL of 0.5 M EDTA was added to stop the reaction. The quenched samples were frozen prior to analysis. A portion of the quenched samples (200 μL) was injected and eluted from a reversed-phase column (Waters RCM or Vydac) using a linear gradient of 5 to 30% acetonitrile in 0.1% TFA. The peaks were recorded using absorbances at 214 and 356 nm.

Equilibrium fluorescence measurements

The fluorescence spectra of the mant nucleotides in the absence and presence of PKA were measured using a Fluoromax spectrofluorimeter equipped with a 500 μL cuvet and holder. Spectra of the nucleotides, PKA, and a mixture of the nucleotides and PKA were measured either by exciting the samples at 290 nm and collecting the emission intensity between 300 and 550 nm or by exciting the samples at 340 nm and collecting the emission intensity between 380 and 550 nm. Excitation and emission slit widths of 1 or 5 nm were used in all experiments. All fluorescence measurements were made in buffers containing 50 mM Mops, pH 7.0, at 25 °C.

Stopped-flow kinetic measurements

All transient kinetic measurements were made using an Applied Photophysics stopped-flow spectrometer. Samples were mixed 1:1 in the instrument cuvet using two identical 2.5 mL syringes. The excitation wavelength was 290 nm, and fluorescence emission was measured using a 420 nm cutoff filter. The instrument collected a total of 400 data points in each experiment and, in some cases, the data were separated with 200 points for the short time frames (0 to 20 ms) and 200 points for the longer time frames (20 to 120–320 ms). For data analysis, the average of 5–10 individual traces was used. The fluorescence data were recorded as volts, and the time data were corrected for the instrument deadtime by adding 1.5 ms to all the time points. Rate constants and amplitudes were obtained by fitting of the data to equations describing a single or double exponential growth/decay using the Applied Photophysics software. Alternatively, the raw data were imported into the computer program KaliedaGraph (Synergy Software, Reading, Pennsylvania) and fit using similar equations. All fluorescence measurements were made in buffers containing 50 mM Mops, pH 7.0, at 25 °C.

Acknowledgments

This work was supported by NIH Grant GM 54846. We would like to thank Dr. Patricia Jennnings, Dr. David Johnson, and John Finkey for help with the equilibrium fluorescence experiments.

References

Adams JA, Taylor SS. 1992. Energetic limits of phosphotransfer in the catalytic subunit of cAMP-dependent protein kinase as measured by viscosity experiments. *Biochemistry 31*:8516–8522.

Adams JA, Taylor SS. 1993. Divalent metal ions influence catalysis and active-site accessibility in the cAMP-dependent protein kinase. *Protein Sci 2*:2177–2186.

Armstrong RN, Kondo H, Granot J, Kaiser ET, Mildvan AS. 1979a. Magnetic resonance and kinetic studies of the manganese(II) ion and substrate complexes of the catalytic subunit of adenosine 3′,5′-monophosphate dependent protein kinase from bovine heart. *Biochemistry 18*:1230–1238.

Armstrong RN, Kondo H, Kaiser ET. 1979b. Cyclic AMP-dependent ATPase activity of bovine heart protein kinase. *Proc Natl Acad Sci USA 76*:722–725.

Bernasconi CF. 1976. *Relaxation kinetics*. New York: Academic Press, Inc. p 288.

Bhatnagar D, Roskoski RJ, Rosendahl MS, Leonard NJ. 1983. Adenosine cyclic 3′-5′-monophosphate dependent kinase: A new fluorescence displacement titration technique for characterizing the nucleotide binding site on catalytic subunit. *Biochemistry 22*:6310–6317.

Chan AC, Kadlecek TA, Elder ME, Filipovich AH, Kuo W-L, Iwashima M, Parslow TG, Weiss A. 1994. ZAP-70 deficiency in an autosomal recessive form of severe combined immunodeficiency. *Science 264*:1599–1601.

Cheng J-Q, Jiang W, Hackney DD. 1998a. Interaction of mant-adenosine nucleotides and magnesium with kinesin. *Biochemistry 37*:5288–5295.

Cheng X, Shaltiel S, Taylor SS. 1998b. Mapping substrate-induced conformational changes in cAMP-dependent protein kinase by protein footprinting. *Biochemistry 37*:14005–14013.

Clauser E, Leconte I, Auzan C. 1992. Molecular basis of insulin resistance. *Horm Res 38*:5–12.

Cohen P. 1999. The development and therapeutic potential of protein kinase inhibitors. *Curr Opin Chem Biol 3*:459–465.

Cook PF, Neville ME, Vrana KE, Hartl FT, Roskoski JR. 1982. Adenosine cyclic 3′,5′-monophosphate dependent protein kinase: Kinetic mechanism for the bovine skeletal muscle catalytic subunit. *Biochemistry 21*:5794–5799.

Elder ME, Lin D, Clever J, Chan AC, Hope TJ, Weiss A, Parslow TG. 1994. Human severe combined immunodeficiency due to a defect in ZAP-70, a T cell kinase. *Science 264*:1596–1599.

Fierke CA, Hammes GG. 1995. Transient kinetic approaches to enzyme mechanisms. *Methods Enzymol 249*:3–37.

Friedman AL, Geeves MA, Manstein DJ, Spudich JA. 1998. Kinetic characterization of myosin head fragments with long-lived myosin.ATP states. *Biochemistry 37*:9679–9687.

Grant B, Adams JA. 1996. Pre-steady-state kinetic analysis of cAMP-dependent protein kinase using rapid quench flow techniques. *Biochemistry 35*:2022–2029.

Hartl FT, Roskoski RJ, Rosendahl MS, Leonard NL. 1983. Adenosine cyclic 3′-5′-monophosphate dependent protein kinase: Interaction of the catalytic subunit and holoenzyme with lin-benzoadenine nucleotides. *Biochemistry 22*:2347–2352.

Hiratsuka T. 1983. New ribose-modified fluorescent analogs of adenine and guanine nucleotides available as substrates for various enzymes. *Biochem Biophys Acta 742*:496–508.

Hoppe J, Freist W, Marutzky R, Shaltiel S. 1978. Mapping the ATP binding site in the catalytic subunit of cAMP-dependent protein kinase; spatial relationship with the ATP binding site of the undissociated enzyme. *Eur J Biochem 90*:427–432.

Johnson KA. 1992. Transient-state kinetic analysis of enzyme reaction pathways. In: Sigman DS, ed. *The enzymes*. San Diego: Academic Press, Inc. pp 2–61.

Knighton DR, Zheng J, Ten Eyck LF, Ashford VA, Xuong N-h, Taylor SS, Sowadski JM. 1991a. Crystal structure of the catalytic subunit of cAMP-dependent protein kinase. *Science 253*:407–414.

Knighton DR, Zheng J, Ten Eyck LF, Xuong N-h, Taylor SS, Sowadski JM. 1991b. Structure of a peptide inhibitor bound to the catalytic subunit of cyclic adenosine monophosphate-dependent protein kinase. *Science 253*:414–420.

Kong C-T, Cook PF. 1988. Isotope partitioning in the adenosine 3′-5′-monophosphate dependent protein kinase reaction indicates a steady-state random kinetic mechanism. *Biochemistry 27*:4795–4799.

Lew J, Taylor SS, Adams JA. 1997. Identification of a partially rate-determining step in the catalytic mechanism of cAMP-dependent protein kinase: A transient kinetic study using stopped-flow fluorescence spectroscopy. *Biochemistry 36*:6717–6724.

Liu X, Pawson T. 1994. Biochemistry of the Src protein-tyrosine kinase: Regulation by SH2 and SH3 domains. *Recent Prog Horm Res 49*:149–160.

Ma Y-Z, Taylor EW. 1997. Kinetic mechanism of a monomeric kinesin construct. *J Biol Chem 272*:717–723.

Madhusudan, Trafny EA, Xuong N-h, Adams JA, Ten Eyck LF, Taylor SS, Sowadski JM. 1994. cAMP-dependent protein kinase: Crystallographic insights into substrate recognition and phosphotransfer. *Protein Sci 3*:176–187.

Mitchell RD, Glass DB, Wong C, Angelos KL, Walsh DA. 1995. Heat stable protein derived peptide substrate analogs: Phosphorylation by cAMP-dependent and cGMP-dependent protein kinase. *Biochemistry 34*:528–534.

Mocz G, Helms MK, Jameson DM, Gibbons IR. 1998. Probing the nucleotide binding sites of axonemal dynein with the fluorescent nucleotide analogue 2′(3′)-O-(-N-methylanthraniloyl)-adenosine 5′-triphosphate. *Biochemistry 37*:9862–9869.

Moyer ML, Gilbert SP, Johnson KA. 1998. Pathway of ATP hydrolysis by monomeric and dimeric kinesin. *Biochemistry 37*:800–813.

Narayana N, Cox S, Xuong N-h, Ten Eyck LF, Taylor SS. 1997. A binary complex of the catalytic subunit of cAMP-dependent protein kinase and adenosine further defines conformational flexibility. *Structure 5*:921–935.

Olah GA, Mitchell RD, Sosnick TR, Walsh DA, Trewhella J. 1993. Solution structure of the cAMP-dependent protein kinase catalytic subunit and its contraction upon binding the protein kinase inhibitor peptide. *Biochemistry 32*:3649–3657.

Pawson T, Scott JD. 1997. Signaling through scaffold, anchoring, and adaptor proteins. *Science 278*:2075–2080.

Rawlings DJ, Saffran DC, Tsukada S, Largaespada DA, Grimaldi JC, Cohen L, Mohr RN, Bazan JF, Howard M, Copeland NG, et al. 1993. Mutation of unique region of Bruton's tyrosine kinase in immunodeficient XID mice. *Science 261*:358–361.

Shaffer J, Adams JA. 1999a. An ATP-linked structural change in protein kinase A precedes phosphoryl transfer under physiological magnesium concentrations. *Biochemistry 38*:5572–5581.

Shaffer J, Adams JA. 1999b. Detection of conformational changes along the kinetic pathway of protein kinase A using a catalytic trapping technique. *Biochemistry 38*:12072–12079.

Thomas JD, Sideras P, Smith CI, Vorechovsky I, Chapman V, Paul WE. 1993. Colocalization of X-linked agammaglobulinemia and X-linked immunodeficiency genes. *Science 261*:355–358.

Torok K, Trentham DR. 1994. Mechanism of 2-chloro-(ϵ-amino-Lys75)-[6-[4-(*N*,*N*-diethylamino)phenyl]-1,3,5-triazin-4-yl]calmodulin interactions with smooth muscle myosin light chain kinase and derived peptides. *Biochemistry 33*:12807–12820.

Woodward S, Eccleston JF, Geeves MA. 1991. Kinetics of the interaction of 2′(3′)-O-(*N*-methylanthraniloyl)-ATP with myosin subfragment 1 and actomyosin subfragment 1: Characterization of two acto-S1-ADP complexes. *Biochemistry 30*:422–430.

Yonemoto W, McGlone ML, Slice LW, Taylor SS. 1991. Prokaryotic expression of the catalytic subunit of cAMP-dependent protein kinase. In: Hunter T, Sefton BM, eds. *Protein phosphorylation (Part A)*. San Diego: Academic Press, Inc. pp 581–596.

Zheng J, Knighton DR, Ten Eyck LF, Karlsson R, Xuong N-h, Taylor SS, Sowadski JM. 1993a. Crystal structure of the catalytic subunit of cAMP-dependent protein kinase complexed with MgATP and peptide inhibitor. *Biochemistry 32*:2154–2161.

Zheng J, Knighton DR, Xuong N-h, Taylor SS, Sowadski JM, Ten Eyck LF. 1993b. Crystal structures of the myristylated catalytic subunit of cAMP-dependent protein kinase reveal open and closed conformations. *Protein Sci 2*:1559–1573.

Zhou J, Adams JA. 1997. Participation of ADP dissociation in the rate-determinig step in cAMP-dependent protein kinase. *Biochemistry 36*:15733–15738.